appliedoptics

Microsphere-assisted super-resolved Mirau digital holographic microscopy for cell identification

Mostafa Aakhte,[1] **Vahid Abbasian,**[1] **Ehsan Ahadi Akhlaghi,**[1,2] **Ali-Reza Moradi,**[2,3,4,*] **Arun Anand,**[5] **and Bahram Javidi**[6]

[1]*Department of Physics, Institute for Advanced Studies in Basic Sciences, P.O. Box 45195-1159, Zanjan, Iran*
[2]*Optics Research Center, Institute for Advanced Studies in Basic Sciences, P.O. Box 45137-66731, Zanjan, Iran*
[3]*Department of Physics, Zanjan, University of Zanjan, P.O. Box 45195-313, Zanjan, Iran*
[4]*Department of Physics, Bilkent University, Cankaya 06800, Ankara, Turkey*
[5]*Applied Physics Department, Faculty of Technology and Engineering, MS University of Baroda, Vadodara 39001, India*
[6]*Department of Electrical and Computer Engineering, University of Connecticut, Storrs, Connecticut 06269-4157, USA*
*Corresponding author: moradika@znu.ac.ir

In this paper, we use a glass microsphere incorporated into a digital holographic microscope to increase the effective resolution of the system, aiming at precise cell identification. A Mirau interferometric objective is employed in the experiments, which can be used for a common-path digital holographic microscopy (DHMicroscopy) arrangement. High-magnification Mirau objectives are expensive and suffer from low working distances, yet the commonly used low-magnification Mirau objectives do not have high lateral resolutions. We show that by placing a glass microsphere within the working distance of a low-magnification Mirau objective, its effective numerical aperture can be increased, leading to super-resolved three-dimensional images. The improvement in the lateral resolution depends on the size and vertical position of microsphere, and by varying these parameters, the lateral resolution and magnification may be adjusted. We used the information from the super-resolution DHMicroscopy to identify thalassemia minor red blood cells (tRBCs). Identification is done by comparing the volumetric measurements with those of healthy RBCs. Our results show that microsphere-assisted super-resolved Mirau DHMicroscopy, being common path and off-axis in nature, has the potential to serve as a benchtop device for cell identification and biomedical measurements.   © 2017 Optical Society of America

OCIS codes: (090.1995) Digital holography; (100.6640) Superresolution; (180.6900) Three-dimensional microscopy; (170.1530) Cell analysis.

https://doi.org/10.1364/AO.56.0000D8

1. INTRODUCTION

Digital holographic microscopy (DHMicroscopy) is an effective technique for non-destructive and non-contact surface profile measurement and quantitative three-dimensional (3D) imaging of phase objects [1–4]. The reconstruction of holograms recorded by a digital sensor is carried out numerically, yielding whole-field information about the object. By introducing a slight angle between the object and the reference waves in the off-axis holography arrangement, the undiffracted reference beam is separated from the virtual and real objects at the reconstruction plane. These arrangements are highly sensitive to environmental vibrations, employ additional optical elements, and lead to higher noise levels. Common-path geometry for interferometric techniques is an elegant arrangement to greatly reduce such uncorrelated phase variations. Recently, a self-referencing common-path geometry for DHMicroscopy

was demonstrated by the use of a Lloyd's mirror configuration [5], by applying lateral shearing through a glass plate [6], and also by a microscope binocular module [7]. Another possibility to provide common-path DHMicroscopy is to employ interferometric objectives, such as a (modified) Michelson objective [8], Linnik [9], and a Mirau objective [10]. The Michelson objectives provide rather longer working distances, wider fields of view, and larger depths of focus, whereas the Mirau microscope objectives (Mirau-MOs) are used in applications requiring higher magnification and numerical apertures. In Mirau interferometry, the interferometric system consists of a single microscope objective, and the reference wave is reflected from a small mirror that is built inside the objective during the manufacturing process.

In optical microscopy, the spatial resolution is confined by the wavelength of the imaging light and the numerical aperture

(NA) of the lens system, due to the restriction imposed by the diffraction limit. In DHMicroscopy, the lateral resolution of the recorded hologram can be determined by the performance of the imaging system and features of the sensor, and the axial resolution is defined by the sensitivity of the detection system to optical path changes [11].

Increasing global interest and rapid growth have been observed for optical super-resolution imaging due to its application benefits in many areas of biology, medicine, and material research. High lateral resolutions can be achieved by synthetically increasing the NA of the detection system. This is done by exchanging the degrees of freedom of the system, such as the object's shape and temporal behavior, wavelength behavior, dimensions, and polarization [12]. One of the earliest approaches for super-resolution by synthetic expansion of an imaging system aperture was based on employing two counter-moving gratings at the input and output planes of the system for immobile objects. The approach was improved by using Dammann and Ronchi gratings, and, recently, by the use of non-periodic spatial masking [13], and binary random masks [14]. These methods can be applied for super-resolution and field-of-view extension in digital holography in a similar way [15–20]. Proper post-processed decoding in the hologram's numerical reconstruction can lead either to a super-resolved image or to an extended field of view.

Recently, super-resolution in imaging by the use of a transparent spherical microlens has shown very promising experimental results [21–23]. A detailed theoretical investigation through vector electromagnetic analysis was recently provided to model the super-resolved imaging process through a microsphere [24]. The model predicts that a perfect spherical micro-particle cannot lead to a sub-100-nm resolution for visible light sources, and an unrevealed mechanism has to be taken into account to explain the reported range of resolution achievements. A super-resolution analysis method has been recently developed which determines the super-resolution values consistent with the resolution definition in classical diffraction-limited optics [23–25]. Super-resolution imaging by the microsphere approach can also be applied to digital holographic microscopy and quantitative phase contrast imaging [26]. In this paper, we consider the microsphere-assisted imaging technique in the common-path DHMicroscopy through a Mirau-MO to acquire super-resolved off-axis holograms. DHMicroscopy through a Mirau arrangement has several advantages, such as stability against environmental and mechanical vibrations, compact optical setup, and easy calibration. However, low-magnification Mirau-MOs do not have high lateral resolution with respect to their vertical resolution, and high-magnification Mirau-MOs are expensive and suffer from low working distances. Here, a technique for super-resolved 3D imaging by a low-magnification Mirau-MO and through the use of a microsphere is described. In spite of conventional microsphere-assisted microscopy techniques, in the present method, the aberration errors can be corrected within the numerical process because the image is obtained via numerical reconstruction and includes the object phase information. In order to prove the capability and usefulness of our approach, we applied it first on a test target and a digital

video disk (DVD) and investigated the various adjustment parameters. Then, we successfully applied the technique to investigate the morphology and volumetric information of cells. As an example, we have used this technique to identify thalassemia red blood cells (tRBCs) from healthy RBCs.

2. EXPERIMENTAL SETUP

Figure 1 shows the setup scheme. An He–Ne laser beam (Pooyafarazma, 632.8 nm, 2 mW) is used as a coherent source. However, to reduce the speckle noise, the spatial coherence of the beam is removed by passing it through a rotating diffuser. The beam is then collimated by the use of lens L1 ($f = 10$ cm) and is sent onto the sample through a cube beam splitter and a Mirau-MO (Nikon, NA 0.3, 10×). A silica microsphere (MS) with a refractive index of 1.46 is mounted at the end of an optical fiber (as a holder), and it is inserted between the Mirau-MO and the sample. Its position is controlled by an x–y–z micro-positioner. Digital holograms are formed by recording the interference pattern of the object beam and the reference beam and were recorded by a digital camera (DCC1545M, Thorlabs, 8-bit dynamic range, 5.2 μm pixel pitch). The object beam is reflected from the object and is transmitted through the MS, the Mirau-MO, and the L2 lens ($f = 16$ cm), and the reference beam is reflected by the built-in small mirror of the Mirau-MO. These two beams are combined at the sensor plane using the L2 lens. The sample was tilted by a small angle (less than 10°) to achieve an off-axis holographic arrangement. The inset of Fig. 1 shows an image of the fiber-connected MS and a magnified scheme of the setup. In the figure, D is the diameter of the inserted MS, and d is the distance between the object and the MS. A standard-resolution target (R3L3S1P, Thorlabs) was used as the first object. Figure 2(a) shows a typical hologram of the sample (Group 7, element 3 of the test target). A reference hologram [Fig. 2(c)] was recorded for phase compensation to remove the system aberrations. The reference hologram was acquired
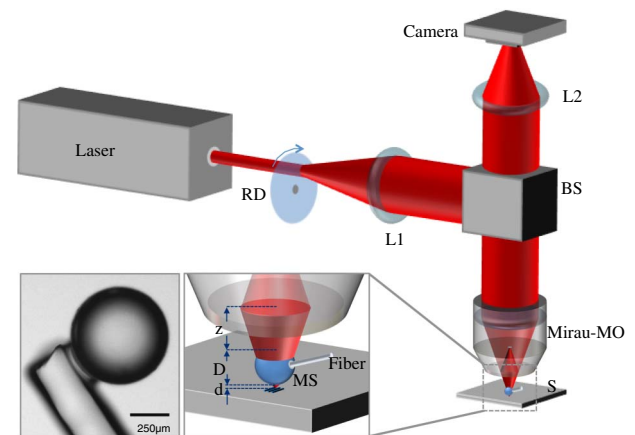
Fig. 1. Scheme of the Mirau-DHMicroscopy setup equipped with a microsphere; RD, rotating diffuser; L1, collimating lens; BS, beam splitter; L2, tube lens; Mirau-MO, Mirau objective; MS, microsphere; S, sample; Inset: image of the fiber connected MS and the magnified scheme of the setup; D, diameter of MS; d, distance between the object and the MS; z, MS-to-Mirau-MO distance.
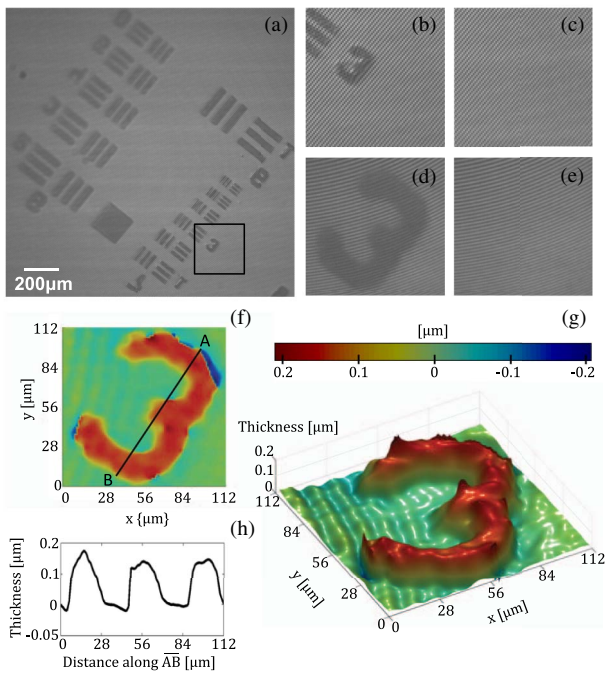
Fig. 2. (a) Hologram of a reflective standard resolution target without inserting an MS. (b) The cropped part of the sample indicated in panel (a) and (c) its associated reference hologram. (d) Hologram of the cropped part after inserting an MS of a 529 μm diameter within the Mirau-MO and sample distance and (e) its reference hologram. (f) The reconstructed two-dimensional thickness profile. (g) The reconstructed 3D thickness profile. (h) One-dimensional thickness profile along the line ($\overline{AB}$) indicated in panel (f).

by taking the element-free area of the test plate as the object. Figures 2(d) and 2(e) show the recorded object and the reference holograms of the same part of the resolution target in the presence of an MS of a 529 μm diameter. The phase and intensity of the reconstructed wavefront can be obtained from the propagated complex wave field of the hologram at the reconstruction plane. We considered the angular spectrum propagation method in scalar diffraction theory for the numerical reconstruction of the holograms [27,28]. The reconstructed phase patterns are unwrapped by Goldstein's branch-cut method to convert them into continuous-phase distributions [29]. Figures 2(f) and 2(g) are the calculated thickness profiles using MS, which is obtained directly from the phase patterns, in two-dimensional and 3D views, respectively. Figure 2(h) is the cross-sectional thickness profile along the line ($\overline{AB}$) indicated in Fig. 2(f). Depending on the relative position of the MS with respect to the Mirau-MO, the sample plane can be adjusted to form a magnified image of the detection system [30]. For any sample-to-Mirau distance, a sharp image is formed exclusively for a specific MS-to-Mirau-MO distance. In the experiments, a hologram of the sample is recorded first without an MS. Then, an MS (with different diameter values) was inserted between the sample and the Mirau-MO. We employed a rotating diffuser in the optical train to reduce the speckle noise. This makes the fringes, however, localized, and recording well-defined and high-contrast interferometric fringes requires fine adjustment of the setup elements.

3. EXPERIMENTAL RESULTS AND DISCUSSIONS

Figure 3(a) shows an atomic force microscope (AFM) image of a DVD with a scanning area of 3 μm × 3 μm. The period of peaks and valleys shown in this figure is 732 ± 41 nm, and the average measured peak to valley height is around 89 ± 5 nm. The DVD structure cannot be resolved by a 10× objective lens (Olympus, NA = 0.3), as shown in Fig. 3(b), but its periodic structure is resolved by a 40× objective (Olympus, NA = 0.75) [Fig. 3(c)]. Nevertheless, microsphere-assisted DHMicroscopy with the 10× Mirau-MO can resolve the DVD structure. Figures 3(d) and 3(e) are the corresponding holograms acquired without and with an MS of a size of 234 μm, respectively. We numerically reconstructed these holograms, obtained the cross-sectional profiles from the corresponding unwrapped phases, and compared the results with the average profile obtained from the AFM image (0101/A, ARA-AFM) [Fig. 3(f)]. The cross-sectional profile is calculated as the average value along several lines perpendicular to the DVD grooves' direction. In Fig. 3(g), the cross-sectional profiles obtained from the reconstruction of the holograms for the two cases without MS and with an MS of $D = 234$ μm are shown. Figure 3(g) (continuous lines) shows that no details of the sample can be retrieved without the MS. However, by
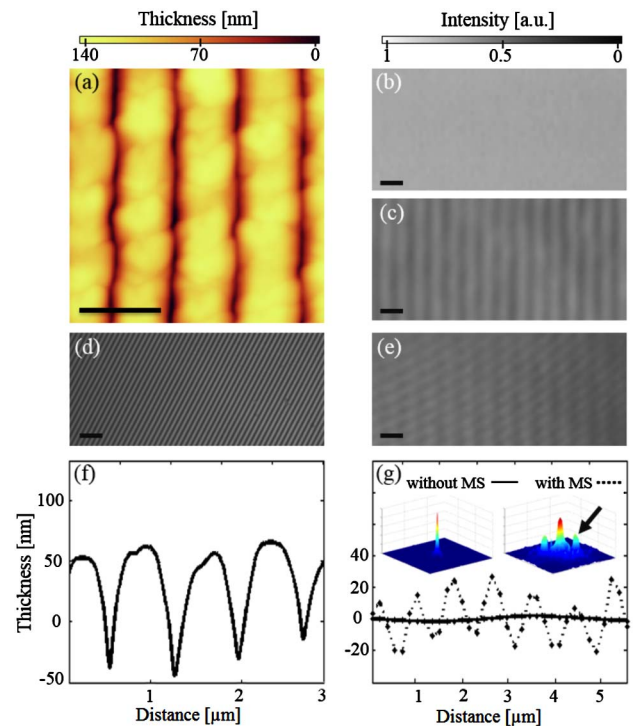

Fig. 3. (a) AFM image of a periodic structure of a DVD. (b) Bright-field microscopy image by a 10× objective. (c) Bright-field microscopy image by a 40× objective. (d) Digital hologram by a 10× Mirau-MO without inserting an MS. (e) Digital hologram by inserting an MS ($D = 234$ μm) within the 10× Mirau-MO and 45× overall magnification. (f) One-dimensional average profile of AFM image. (g) One-dimensional profiles obtained from hologram reconstruction; inset: Fourier spectrum of the reconstructed thickness map. Scale bar in all panels is 1 μm.

introducing the MS, the resolution is increased, so the periodic structure of the DVD becomes visible. From the MS-assisted DHMicroscopy, the measured peaks and valleys' average period was 728 ± 50 nm, which is in good agreement with the information provided by the AFM image. Resolving the periodic DVD structure in the MS-assisted case is also confirmed by the Fourier spectra of the obtained phase maps, which are shown in the inset of Fig. 3(g). The DVD periodic structure is distinguished as a sharp frequency sideband in the Fourier domain for the hologram using the MS (as indicated by an arrow). However, sidebands due to the periodic structure of the DVD are not visible for the case without the MS. The measured average peak to valley height from DHMicroscopy is 34 ± 7 nm. Due to the DVD's sharp-edge structure, matching the AFM measurement of the average peak to valley height needs even higher resolutions for the holographic imaging system. Nevertheless, in more commonly used samples, including biomaterials, height profiles variations are usually smooth, and this artifact may be less pronounced.

The classic definition of spatial resolution, based on the concept of the point-spread function (PSF), may be used to evaluate the resolution enhancement factor introduced by the MS [31]. The introduction of the MS increases the imaging system's effective NA value, and, according to the intrinsic relation between the NA and the PSF size, it leads to a higher resolution. In our microscopy system, the image plane and the tube lens remain fixed during the experiments, and repositioning of the MS toward the Mirau-MO allows for a higher magnification factor. On the other hand, this increases the MS collection cone and the complete system's effective NA value. Therefore, the resolution evaluation can be performed by measuring the magnification factor gained by introducing the MS.

Figure 4 shows the experimental results of the lateral magnification and the field-of-view change in improved-resolution digital holography as a function of the MS diameter and position. The vertical axis represents the magnification improvement by introducing the MS. As classical optics predicts, the magnification decreases when the MS-to-Mirau-MO distance (z) increases. However, beyond a maximum distance (z_0), the imaging system cannot form a clear image anymore. The horizontal axis of Fig. 4 is the relative position of the MS, defined as $\Delta z = z_0 - z$. The results corresponding to three different MS sizes ($D \sim 100$ μm, $D \sim 234$ μm, and $D \sim 529$ μm) among several tested MSs are shown. The magnification improvement has a linear dependence with the position of the inserted MS. The results represent that for smaller MSs, the final magnification has greater sensitivity to its position.

The possibility to vary the size and position of the inserted MS allows us to obtain a large range of magnification factors. The combination of the MS and the Mirau-MO can be considered as a single microscope objective. For each MS, we observed that high-contrast interferometric fringes and a clear image formation can be obtained if Δz is approximately less than $2D$. Therefore, the highest magnification for each MS can be obtained at $\Delta z \sim 2D$. Both the fringe contrast and the sharpness of the images are decreased when Δz is increased. Acquiring the same magnification enhancement can be
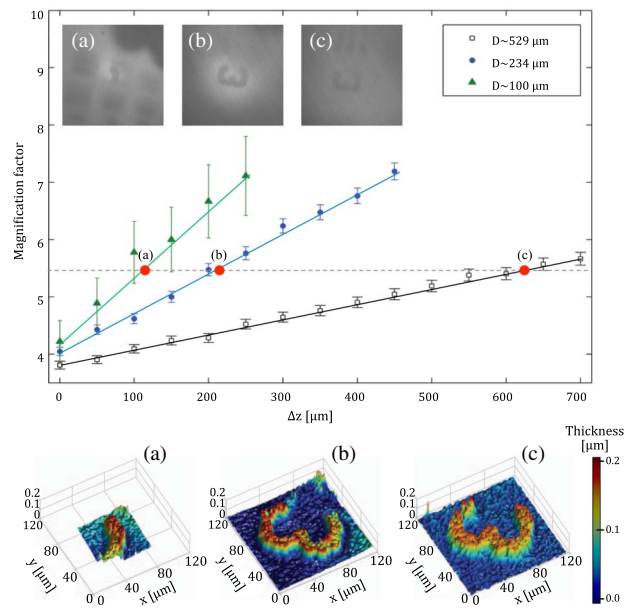
Fig. 4. Magnification factor for three silica MSs of $D \sim 100$ μm, $D \sim 234$ μm, and $D \sim 529$ μm sizes versus their relative positions to the Mirau-MO. Final magnification is obtained by multiplication of this factor and the system's magnification without an MS. The dashed line indicates a factor of 5.5 that can be obtained with all of the MSs by properly positioning them between the Mirau-MO and the sample. $D \sim 100$ μm at $\Delta z = 115$ μm, $D \sim 234$ μm at $\Delta z = 215$ μm, or $D \sim 529$ μm at $\Delta z = 625$ μm, indicated by red dots (a), (b), and (c) on the dashed line, respectively. The corresponding recorded holograms are shown in the inset of the plot, and their reconstructed 3D profiles are shown in the bottom of the figure.

provided by the use of any of the above-mentioned MSs; as shown, for example, for ~5.5 enhancement in the plot of Fig. 4 [indicated by (a), (b), and (c)]. However, as the sample holograms in the insets show, the resulting holograms may differ in terms of the effective field of view and the fringe contrast. The associated reconstructed 3D images are also shown in Fig. 4. The magnification factor was calculated by averaging its values along several lines, similar to the $\overline{AB}$ line in Fig. 2(f), for each reconstructed hologram. Due to the limitation imposed by the field of view, the length of the $\overline{AB}$ line covers smaller numbers of pixels in higher magnifications. Hence, the averaging values have higher error bars. The resolutions in the longitudinal and lateral directions are decoupled in this system. Hence, the increase in the resolution in lateral directions by inserting an MS between the Mirau-MO and the object will not alter the resolution in the longitudinal direction, as illustrated in Figs. 4(a)–4(c). By digitally processing the holographic pattern at different depths, the intensity image of the sample under study can be reconstructed. The numerical refocusing capability may be used for a synthetic extension of the image depth of field, which is useful, for instance, in biomaterial imaging.

We further observed that placing the MS in immersion oil substantially increases the effective magnification. We injected a thin layer of oil between the MS and the sample. The improved resolution of the microsphere-assisted imaging

technique is related to the enhancement of the effective NA of the system due to the reduction of the wavelength of light in the medium and the enhancement of the collection cone of the objective lens. Our observations are in agreement with previous studies for super-resolution imaging through embedding high refractive index MSs within transparent elastomers [32].

We then demonstrated the use of our setup in 3D imaging and identification of biological samples. Blood samples were collected from a healthy subject and from a subject who tested positive for thalassemia minor. Thalassemia is an inherited blood disorder in which the body creates hemoglobin with an abnormal form [33,34]. There are different types of thalassemia diseases, and each one includes thalassemia major and thalassemia minor forms. Thalassemia minor occurs if one receives the faulty gene from only one parent. In medical laboratories, a complete blood count (CBC) test may reveal anemia, and a hemoglobin electrophoresis test can show the presence of abnormal hemoglobin forms. tRBCs are known to appear small and abnormally shaped under the microscope. However, the volumetric measurement of a single-cell morphology may provide a more precise identification of tRBCs in relation to normal ones, which can be obtained using DHMicroscopy experiments [35]. Figures 5(a) and 5(b) show holograms of RBCs that were recorded without and with an MS ($D \sim 234$ μm) in the Mirau-DHMicroscopy system, respectively. Figures 5(c) and 5(d) are the associated phase patterns obtained from the reconstructed holograms after subtracting the background phase information obtained from the corresponding reference holograms for a normal RBC and for a tRBC, respectively. As can be seen, the phase of the RBC and the rest of the field of view have different value ranges. Since the phase difference is a function of both the thickness and refractive index of the sample under study, changes in both can be revealed by phase changes. However, we assume here negligible changes for the refractive index, so the phase changes are due to the variations in the RBC thickness. By a simple grayscale-to-binary transformation of the phase maps, the surface covered by any RBC can

be assessed. The cross-sectional thickness profile along any arbitrary line across the cells can also be calculated, and hence, the volume of the cells can be obtained. For normal RBC differentiation from tRBC, we recorded a large number of holograms from RBCs with an MS and calculated the corresponding volume of several cells in each sample. The volume of RBCs was calculated following the method explained in [36]. Figure 5(e) shows the final volume of about 140 RBCs (from normal and thalassemia ones), demonstrating the visible contrast between the two types, even for this limited number of cells, which may not be achieved by the use of a conventional high-magnification microscopes or through a CBC test. Figure 5(f) is the histogram of the volume distribution of the cells, which shows the predicted volume distribution by a quick observation.

From the recorded holograms for large numbers of cells, further measurements can also be obtained, e.g., the roughness of the cell membranes, thickness distribution behavior, cell circularity, volumetric aspect ratio, and cell convexity, to name a few. These parameters can serve as identification parameters for further study of the effect of important organic compounds on the structural properties of cells. However, for the current case, considering the changes in volume of the cells has shown to be sufficient to discriminate tRBCs from normal RBCs.
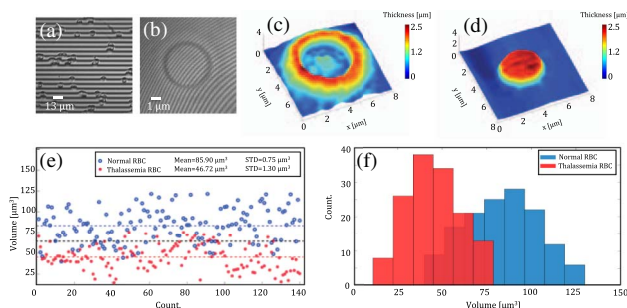
4. CONCLUSION

We have experimentally demonstrated a super-resolved common-path DHMicroscopy by using a glass MS placed within the working distance of a Mirau-MO and showed its capability for cell identification purposes. This arrangement offers a vibration-immune and compact apparatus to perform 3D imaging with a high resolving power. The improvement in the lateral resolution depends on the size and the vertical position of the microsphere, and by varying these parameters, the system resolution and magnification can be adjusted. We observed that imaging with a bigger MS has a wider field of view, but the magnification improvement factor is less sensitive to the MS vertical position. Therefore, according to the imaging conditions, a proper MS size may be chosen. We tested the setup using a commercial test target and also a DVD surface. Further, we successfully used the information from the DHMicroscopy to identify tRBCs through volumetric measurements of cells. Our microsphere-assisted DHMicroscopy approach may be applied to a variety of DHMicroscopy arrangements to improve the resolution [37], and it has the potential to become a benchtop apparatus for biomedical measurements.

Fig. 5. (a) Hologram of RBC sample without using MS in Mirau-DHMicroscopy setup. (b) Hologram of an RBC with MS-assisted Mirau-DHMicroscopy ($D \sim 234$ μm). (c) 3D Phase map of a normal RBC and (d) tRBC from hologram reconstruction. (e) Final volume of about 140 RBCs from normal (blue) and thalassemia (red) samples. (f) Histogram of the volume distribution of the normal and tRBCs. The blue and red dashed lines in Fig. 5(e) show the mean value of the normal and tRBCs' volume, respectively. The black dashed line shows the average volume of all the samples, which can be taken as a discrimination threshold.

REFERENCES

1. U. Schnars and W. Jueptner, *Digital Holography: Digital Hologram Recording, Numerical Reconstruction, and Related Techniques* (Springer-Verlag, 2005).
2. W. Osten, A. Faridian, P. Gao, K. Körner, D. Naik, G. Pedrini, A. K. Singh, M. Takeda, and M. Wilke, "Recent advances in digital holography," Appl. Opt. **53**, G44–G63 (2014).

3. I. Moon, M. Daneshpanah, A. Anand, and B. Javidi, "Cell identification computational 3-D holographic microscopy," Opt. Photon. News **22**(6), 18–23 (2011).

4. E. Cuche, F. Bevilacqua, and C. Depeursinge, "Digital holography for quantitative phase-contrast imaging," Opt. Lett. **24**, 291–293 (1999).

5. V. Chhaniwal, A. S. Singh, R. A. Leitgeb, B. Javidi, and A. Anand, "Quantitative phase-contrast imaging with compact digital holographic microscope employing Lloyd's mirror," Opt. Lett. **37**, 5127–5129 (2012).

6. A. S. G. Singh, A. Anand, R. A. Leitgeb, and B. Javidi, "Lateral shearing digital holographic imaging of small biological specimens," Opt. Express **20**, 23617–23622 (2012).

7. S. Ebrahimi, A. R. Moradi, A. Anand, and B. Javidi, "Digital holographic microscopy with coupled optical fiber trap for cell measurement and manipulation," Opt. Lett. **39**, 2916–2919 (2014).

8. P. J. de Groot and J. F. Biegen, "A new class of wide-field objectives for 3D interference microscopy," Proc. SPIE **9525**, 95250N (2015).

9. R. Guo, B. Yao, J. Min, M. Zhou, X. Yu, M. Lei, S. Yan, Y. Yang, and D. Dan, "LED-based digital holographic microscopy with slightly off-axis interferometry," J. Opt. **16**, 125408 (2014).

10. M. Leon-Rodriguez, R. Rodriguez-Vera, J. A. Rayas, and S. Calixto, "Digital holographic microscopy through a Mirau interferometric objective," Opt. Laser Eng. **51**, 240–245 (2013).

11. P. Marquet, B. Rappaz, P. J. Magistretti, E. Cuche, Y. Emery, T. Colomb, and C. Depeursinge, "Digital holographic microscopy: a noninvasive contrast imaging technique allowing quantitative visualization of living cells with subwavelength axial accuracy," Opt. Lett. **30**, 468–470 (2005).

12. M. Martínez-Corral and G. Saavedra, "The resolution challenge in 3D optical microscopy," Prog. Opt. **52**, 1–67 (2009).

13. A. Borkowski, Z. Zalevsky, and B. Javidi, "Geometrical super resolved imaging using nonperiodic spatial masking," J. Opt. Soc. Am. A **26**, 589–601 (2009).

14. A. Borkowski, Z. Zalevsky, E. Marom, and B. Javidi, "Enhanced geometrical super resolved imaging with moving binary random mask," J. Opt. Soc. Am. A **28**, 566–575 (2011).

15. M. Martinez-Corral, A. Pons, and M. T. Caballero, "Axial apodization in 4π-confocal microscopy by annular binary filters," J. Opt. Soc. Am. A **19**, 1532–1536 (2002).

16. M. Paturzo, F. Merola, S. Grilli, S. De Nicola, A. Finizio, and P. Ferraro, "Super-resolution in digital holography by a two-dimensional dynamic phase grating," Opt. Express **16**, 17107–17118 (2008).

17. P. Ferraro and M. Paturzo, "Correct self-assembling of spatial frequencies in super-resolution synthetic aperture digital holography," Opt. Lett. **34**, 2787–3652 (2009).

18. Z. Zalevsky, E. Gur, J. Garcia, V. Micó, and B. Javidi, "Superresolved and field-of-view extended digital holography with particle encoding," Opt. Lett. **37**, 2766–2768 (2012).

19. Y. Cotte, F. Toy, P. Jourdain, N. Pavillon, D. Boss, P. Magistretti, P. Marquet, and C. Depeursinge, "Marker-free phase nanoscopy," Nat. Photonics **7**, 113–117 (2013).

20. E. Sánchez-Ortiga, M. Martinez-Corral, G. Saavedra, and J. Garcia-Sucerquia, "Enhancing spatial resolution in digital holographic microscopy by biprism structured illumination," Opt. Lett. **39**, 2086–2089 (2014).

21. Z. Wang, W. Guo, L. Li, B. Luk'yanchuk, A. Khan, Z. Liu, Z. Chen, and M. Hong, "Optical virtual imaging at 50 nm lateral resolution with a white-light nanoscope," Nat. Commun. **2**, 218 (2011).

22. A. Darafsheh, N. I. Limberopoulos, J. S. Derov, D. E. Walker, and V. N. Astratov, "Advantages of microsphere-assisted super-resolution imaging technique over solid immersion lens and confocal microscopies," Appl. Phys. Lett. **104**, 061117 (2014).

23. K. W. Allen, N. Farahi, Y. Li, N. I. Limberopoulos, D. E. Walker, Jr., A. M. Urbas, V. Liberman, and V. N. Astratov, "Super-resolution microscopy by movable thin-films with embedded microspheres: resolution analysis," Ann. Phys. **527**, 513–522 (2015).

24. Y. Duan, G. Barbastathis, and B. Zhang, "Classical imaging theory of a microlens with super-resolution," Opt. Lett. **38**, 2988–2990 (2013).

25. K. W. Allen, N. Farahi, Y. Li, N. I. Limberopoulos, D. E. Walker, A. M. Urbas, and V. N. Astratov, "Overcoming the diffraction limit of imaging nanoplasmonic arrays by microspheres and microfibers," Opt. Express **23**, 24484–24496 (2015).

26. Y. Wang, S. Guo, D. Wang, Q. Lin, L. Rong, and J. Zhao, "Resolution enhancement phase-contrast imaging by microsphere digital holography," Opt. Commun. **366**, 81–87 (2016).

27. J. W. Goodman, *Introduction to Fourier Optics* (McGraw-Hill, 2005).

28. A. Anand, V. K. Chhaniwal, and B. Javidi, "Real time digital holographic microscopy for phase contras 3D-imaging of dynamic phenomena," J. Disp. Technol. **6**, 500–505 (2010).

29. R. M. Goldstein, H. A. Zebker, and C. Werner, "Satellite radar interferometry: two-dimensional phase unwrapping," Radio Sci. **23**, 713–720 (1988).

30. R. Ye, Y. Ye, H. F. Ma, L. Cao, J. Ma, F. Wyrowski, R. Shi, and J. Zhang, "Experimental imaging properties of immersion microscale spherical lenses," Sci. Rep. **4**, 3769 (2014).

31. S. M. Mansfield, W. R. Studenmund, G. S. Kino, and K. Osato, "High-numerical-aperture lens system for optical storage," Opt. Lett. **18**, 305–307 (1993).

32. A. Darafsheh, C. Guardiola, A. Palovcak, J. C. Finlay, and A. Cárabe, "Optical super-resolution imaging by high-index microspheres embedded in elastomers," Opt. Lett. **40**, 5–8 (2015).

33. K. Yazdanbakhsh, C. Lomas-Francis, and M. E. Reid, "Blood groups and diseases associated with inherited abnormalities of the red blood cell membrane," Transfus. Med. Rev. **14**, 364–374 (2000).

34. D. J. Weatherall, "Pathophysiology of thalassemia," Baillieres Clin. Haematol. **11**, 127–146 (1998).

35. B. Javidi, I. Moon, S. K. Yeom, and E. Carapezza, "Three-dimensional imaging and recognition of microorganism using single-exposure on-line (SEOL) digital holography," Opt. Express **13**, 4492–4506 (2005).

36. K. Jaferzadeh and I. Moon, "Quantitative investigation of red blood cell three-dimensional geometric and chemical changes in the storage lesion using digital holographic microscopy," J. Biomed. Opt. **20**, 111218 (2015).

37. P. Memmolo, V. Bianco, F. Merola, L. Miccio, M. Paturzo, and P. Ferraro, "Breakthroughs in photonics 2013: holographic imaging," IEEE Photon. J. **6**, 1–6 (2014).